Electron capture in collisions of Al^{2+} ions with He atoms at intermediate energies

A. Watanabe and H. Sato*
Department of Information Sciences, Ochanomizu University, Tokyo 112-8610, Japan

J. P. Gu, G. Hirsch, and R. J. Buenker
Theoretische Chemie, Bergische Universität–GesamthochschuleWuppertal, D-42097 Wuppertal, Germany

M. Kimura
Graduate School of Science and Engineering, Yamaguchi University, Ube 755-8611, Japan
(Received 8 February 2001; published 20 August 2001)

Electron capture resulting from collisions of Al^{2+} ions with He atoms from 0.15 to 1000 keV/u is investigated using a molecular-orbital representation within a semiclassical frame. Molecular electronic states and corresponding couplings are determined by the ALCHEMY program. Sixteen molecular states all connecting to single-electron-capture processes are included, and hence radial and rotational couplings among these channels are fully considered. The trajectory effect arising from the straight-line, Coulomb, and ground-state potential trajectories for electron-capture and excitation processes is carefully assessed. The electron-capture cross section by ground-state $Al^{2+}(^2S)$ ions slowly increases before it reaches a maximum of $1.3\times10^{-16}\,cm^2$ at 100 keV/u. Those for metastable $Al^{2+}(^2P)$ ions sharply increase with increasing energy, and reach a peak at 1 keV/u with a value of $1.5\times10^{-16}\,cm^2$. The earlier experimental data are found to be larger by an order of magnitude although their energy dependence is in good accord with the present result. Excitation cross sections for both the ground and metastable states are found to be much larger by a factor of 2–3 than corresponding capture cross sections above 1 keV/u although they become comparable below this energy.

DOI: 10.1103/PhysRevA.64.032717 PACS number(s): 34.70.+e, 34.50.−s, 34.10.+x

I. INTRODUCTION

Electron capture resulting from collisions of multiply charged ions of heavy atoms ($Z>10$) with neutral species plays a significant role in applications such as medical treatment, fusion plasma, astrophysics, thin-film manufacturing, and laboratory plasmas in addition to its fundamental interest in atomic physics. However, theoretical and experimental studies to understand the structures and dynamics involving these ions are scarce due partly to the difficulty of ion production for experiments and of the structural determination of many-electron systems for theory. We have been concerned with heavier ($Z>10$) projectiles and targets in our previous theoretical studies, and rigorous investigations have been carried out for single- and double-electron capture by multiply charged ions of heavy atoms in the third row of the periodic table such as Si, P, and S, from H and He targets over the years, in conjunction with various applications [1–5]. These studies have provided a basic understanding of scattering dynamics for heavy ions as well as accurate cross-section data for inelastic processes at intermediate energies. As a continuation of this work, we have considered Al ions in this study, since Al is one of the most abundant atomic species, and hence it is involved in a variety of phenomena in nature. This atom is also the last one we have not examined among third-row species in the periodic table. But this ion is of importance in applications since aluminum atoms and ions have been one of the most important atomic species in various applied fields. In recent years, they have become increasingly important for high-technology areas such as Al thin-film manufacturing based on ion-beam technology, and hence accurate information on the cross sections for inelastic processes and their dynamics is very much required for simulation studies. We intend to provide the cross-section data for single-electron capture and excitation in a wide range of collision energies.

The particular reactions we are concerned with are single-electron-capture processes by the following:

(i) the ground-state Al ion

$$Al(^2S)^{2+}+He\rightarrow Al(^1S,^3P,^1P,^1D,^3S)^{+}+He^{+}, \tag{1}$$

(ii) the excited-state Al ion

$$Al(^2P)^{2+}*+He\rightarrow Al^{+}+He^{+}. \tag{2}$$

There has been one experimental attempt to measure electron capture for the process (1) is this system in the energy region 0.5–8 keV [6], in which the energy region overlaps with ours, thus enabling a direct comparison. In this study, we have employed a close-coupling approach based on a molecular-orbital expansion method (MO-CC) within a semiclassical frame for the scattering dynamics [7], and adiabatic potentials and nonadiabatic coupling matrix elements are computed with the configuration-interaction (ALCHEMY) method [8]. But the multireference single- and double-excitation configuration interaction (MRD-CI) method [9] is also adopted to carry out a comparative study of the electronic states by two different methods. In addition, a small-scale dynamical calculation based on a fully quantal approach has also been carried out to examine the semiclassical result.

*Also at Graduate School of Humanities and Sciences, Ochanomizu University, Tokyo 112-8610, Japan.

TABLE I. Number of reference configurations N_{ref} and number of roots N_{root} treated in each irreducible representation and corresponding number of generated (N_{lot}) and selected (N_{sel}) symmetry-adapted functions for a threshold of 1.5×10^{-7} hartrees at $R=3.2a_0$. Note that R is the internuclear distance between Al^{2+} and He.

State	$N_{\mathrm{ref}}/N_{\mathrm{root}}$	N_{lot}	N_{sel}
$^2A_1$	44/8	3 044 094	143 213
$^2B_1$	26/5	2 407 020	779 89
$^4A_1$	28/2	2 811 694	104 388
$^2B_1$	26/2	2 761 433	95 807

II. THEORETICAL MODEL

A. Molecular states

The adiabatic potential curves of $[AlHe^{2+}]$ and corresponding coupling matrix elements are obtained by employing two different approaches, both within the *ab initio* configuration-interaction framework. The first approach is the multireference single- and double-excitation configuration-interaction method [9] with configurations selected for a threshold larger than 1.5×10^{-7} hartree and energy extrapolation, using the TABLE CI algorithm [10]. The two electrons in the first (lowest) molecular orbital are kept inactive in the present CI calculation, and the highest MO is discarded. The coupling matrix elements are calculated by using the resulting CI wave functions. The radial coupling elements are calculated by using a finite-difference method [11]. In these calculations, the basis set for the aluminum atom is $(15s10p5d2f)$, contracted to $[11s7p4d1f]$ [12], where atomic-orbital basis functions are employed that are fixed linear combinations of single (primitive) Cartesian Gaussians. But the exponent of the *f* function has been reoptimized and the value obtained is 0.34; the *s,p* basis set is from [13]. For the He atom, the $(10s5p1d)/[7s4p1d]$ basis set is employed [14], but the most diffuse *d* function with an exponent of 0.03 is deleted. Further details of our *ab initio* MRD-CI calculations are listed in Table I.

The second approach is based on the ALCHEMY [8] program, in which the ten electrons on 3σ and 1π orbitals are frozen, while the three electrons in 16σ, 5π, and 2δ orbitals are treated as active. Slater-type orbitals (STOs) are employed and all orbitals up to $n=3$ and partly up to $n=4$ manifolds for the Al atom are included, while only $1s$ STOs are considered for the He atom [15]. The Slater exponents used are given in Table II.

As shown below, the MRD-CI method gives better absolute precision for asymptotic energies compared to those from ALCHEMY. However, we have found that a much larger basis set is needed to obtain high-lying levels by this method, and hence we have employed the alternative ALCHEMY program for this purpose, whose results are somewhat less accurate. In order to examine the two methods, we have carried out scattering calculations by using two sets of MOs and compared the results as described in detail below.

TABLE II. The STO exponents.

	Al		He
$1s$	14.226 90, 10.726 10	$1s$	1.417 14, 2.376 82, 4.376 28,
$2s$	5.003 60, 3.631 24		6.526 99, 7.942 52
$3s$	1.773 96, 1.107 66		
$4s$	0.600 00, 0.400 00		
$2p$	7.207 81, 3.654 13		
$3p,3d$	1.682 75, 0.913 81		

B. Scattering dynamics

1. Semiclassical approach

A semiclassical MO expansion method with a straight-line trajectory of the incident ion was employed to study the collision dynamics above 30 eV [7]. In this approach, the relative motion of heavy particles is treated classically, while electronic motions are treated quantum mechanically. The total scattering wave function was expanded in terms of products of a molecular electronic state and atomic-type electron translation factors (ETFs) [7], in which the inclusion of the ETF satisfies the correct scattering boundary condition. Substituting the total wave function into the time-dependent Schrödinger equation and retaining the ETF correction up to the first order in the relative velocity between the collision partners, we obtain a set of first-order coupled equations in time *t*. Transitions between the molecular states are driven by nonadiabatic couplings. By solving the coupled equations numerically, we obtain the scattering amplitudes for transitions: the square of the amplitude gives the transition probability, and integration of the probability over the impact parameter gives the cross section. The molecular states included in the dynamical calculations are 16 in number (see Fig. 1 below), separating into the ground-state channel $[Al^{2+}+He(^1S),\ 1\ ^2\Sigma]$, single-capture channels $[Al^+(^1S)+He^+,\ 2\ ^2\Sigma]$, $[Al^+(^3P)+He^+,\ 4\ ^2\Sigma,2\ ^2\Pi]$, $[Al^+(^1P)+He^+,\ 5\ ^2\Sigma,3\ ^2\Pi]$, $[Al^+(^1D)+He^+,\ 8\ ^2\Sigma,\ 5\ ^2\Pi,2\ ^2\Delta]$, and $[Al^+(^3S)+He^+,\ 9\ ^2\Sigma]$, and excitation channels $[Al^{2+}(^2P)+He,\ 3\ ^2\Sigma,1\ ^2\Pi]$, $[Al^{2+}(^2D)+He,\ 6\ ^2\Sigma,4\ ^2\Pi,1\ ^2\Delta]$, and $[Al^{2+}(^2S)+He,\ 7\ ^2\Sigma]$. The initial channels for electron capture by the metastable ions correspond to $[Al^{2+}(^2D)+He,\ 6\ ^2\Sigma,4\ ^2\Pi,1\ ^2\Delta]$.

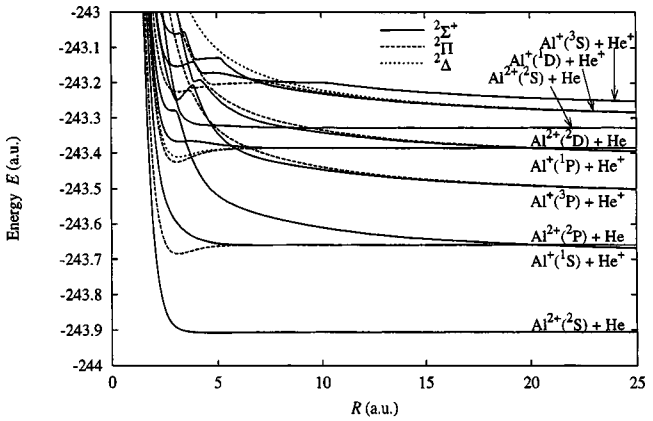

FIG. 1. Adiabatic potentials for $[AlHe^{2+}]$.

TABLE III. Comparison of asymptotic energies for the $[AlHe^{2+}]$ system.

Asymptote	Relative energy (eV) ALCHEMY	MRD-CI	Experiment [17]
$Al^{2+}(^2S)+He$ $1\ ^2\Sigma$	0	0	0
$Al^{+}(^1S)+He^{+}$ $2\ ^2\Sigma$	5.3740	5.7988	5.7596
$Al^{2+}(^2P)+He$ $3\ ^2\Sigma,\ 1\ ^2\Pi$	6.7127	6.6593	6.6557
$Al^{+}(^3P)+He^{+}$ $4\ ^2\Sigma,\ 2\ ^2\Pi$	9.9589	10.4156	10.3956
$Al^{+}(^1P)+He^{+}$ $5\ ^2\Sigma,\ 3\ ^2\Pi$	12.8132	13.2289	13.1801
$Al^{2+}(^2D)+He$ $6\ ^2\Sigma,\ 4\ ^2\Pi,\ 1\ ^2\Delta$	14.1546	14.3772	14.3764
$Al^{2+}(^2S)+He$ $7\ ^2\Sigma$	15.7219		15.6420
$Al^{+}(^1D)+He^{+}$ $8\ ^2\Sigma,\ 5\ ^2\Pi,\ 2\ ^2\Delta$	15.8308		16.3571
$Al^{+}(^3S)+He^{+}$ $9\ ^2\Sigma$	16.6879		17.0759

Although it is known that the trajectory effect for electron capture is important particularly for lower collision energies [16], it appears that a detailed quantitative study of this effect is still lacking. Therefore, in the present work, we examine this effect carefully for individual channels by using a straight-line trajectory, a Coulomb trajectory, and that arising from the ground-state potential in order to quantify it as a function of collision energy. Furthermore, these results are also compared with that of a fully quantum-mechanical calculation as described below.

2. Quantum approach

A fully quantum-mechanical representation of the MO expansion method was employed; that is, the total wave function is expanded in products of molecular electronic and nuclear wave functions and ETFs, and is substituted into a time-independent Schrödinger equation to yield a set of second-order coupled equations [7]. By solving the coupled equations numerically, the scattering S matrix is extracted. From the conventional treatment, the S matrix can be obtained to derive the transition probability and hence the cross section. The four MOs included in the present calculation are the initial ground-state channel $[Al^{2+}(^2S)+He]$, the electron-capture channel $[Al^{+}(^1S)+He^{+},2\ ^2\Sigma]$, and excitation channels $[Al^{2+}(^2P)+He,3\ ^2\Sigma,1\ ^2\Pi]$.

III. RESULTS AND DISCUSSIONS

A. Adiabatic potentials and coupling matrix elements

The present adiabatic potential curves including capture and excitation channels for Σ, Π, and Δ states based on ALCHEMY are illustrated in Fig. 1. The precision of the present calculations by two approaches is tabulated in Table III along with experimental data [17]. Corresponding asymptotes are also included in the table. The asymptotic $1\ ^2\Sigma$ state corresponds to the initial $[Al^{2+}(^2S)+He(^1S)]$ channel. $2\ ^2\Sigma$ and $3\ ^2\Sigma$ have an avoided crossing at around $20a_0$, and beyond this R they switch their character. Projectile-ion excitation and electron-capture channels appear alternately within a few eV width as the energy goes up, and this suggests that the projectile excitation states may play an important role for electron capture. Hence, we look carefully at their role as well as capture from excitation channels.

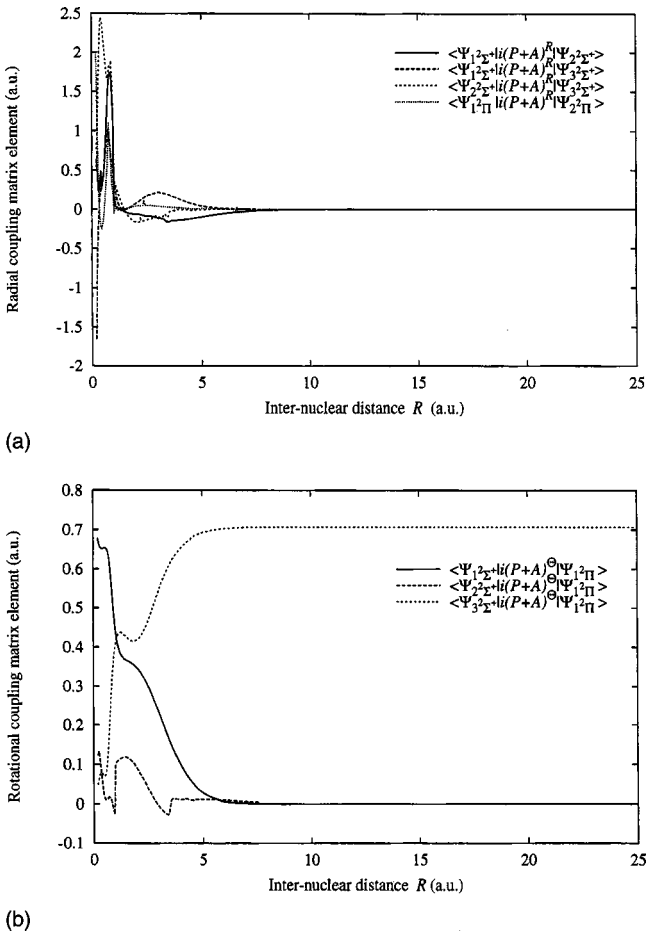

FIG. 2. Representative (a) radial and (b) angular couplings.

Representative matrix elements for both radial and rotational couplings are displayed in Figs. 2(a) and 2(b), respectively. The most important radial coupling matrix elements that connect the $1\ ^2\Sigma$ and $2\ ^2\Sigma$ states are of relatively short range, insignificant beyond $\sim 8a_0$. The rotational coupling between $3\ ^2\Sigma$ and $1\ ^2\Pi$ goes to a constant in the asymptotic region because they are degenerate states. Similar short-range trends prevail for couplings among low to intermediate levels. Although they become somewhat longer in range for higher levels, most of them are found to apparently diminish beyond $10a_0$. Therefore, we restrict our scattering calculation within the range of $20a_0$. Couplings that connect the $1\ ^2\Sigma$ and $2\ ^2\Sigma$ states to higher capture states are found to be weak, and the direct formation of excited states is unlikely. Rotational couplings reflect the nature of the adiabatic potentials and hence are also of short range.

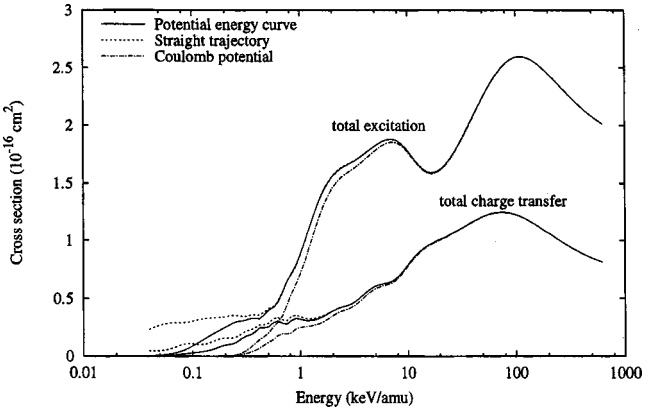

FIG. 3. Electron-capture and excitation cross sections for three different trajectories: the straight-line, Coulomb, and ground-state potential trajectories.

B. Dynamics

1. Comparison between two sets of MOs

We have conducted a comparative study to examine the two sets of MOs in the electron-capture process. In the calculation, we have been concerned with electron capture by the ground-state ion only, and adopted the semiclassical MO-CC method with inclusion of six MOs from the ground state, i.e., $1\,^2\Sigma - 4\,^2\Sigma$, $1\,^2\Pi$, and $2\,^2\Pi$ obtained by ALCHEMY and a MRD-CI calculation. At the collision energy 1 keV/u, capture cross sections to $[\mathrm{Al}^+(^1S)+\mathrm{He}^+,2\,^2\Sigma]$ by the two sets are found to agree within 5%, although the agreement between the two cross sections to the higher level $[\mathrm{Al}^+(^3P)+\mathrm{He}^+,4\,^2\Sigma,2\,^2\Pi]$ becomes slightly less satisfactory (within 8%). This situation is essentially unchanged even if the collision energy increases to 10 keV/u or decreases to the lowest energy of 0.15 keV/u. Therefore, the difference between the two sets of MOs is considered to be not very significant for determination of scattering dynamics, and the present ALCHEMY results are sufficiently accurate for the qualitative and quantitative discussions below.

2. Trajectory effects

In this subsection, before beginning the detailed discussion of electron capture, we need to assess the trajectory effect. In Fig. 3, the cross sections for electron capture and excitation in collisions of the ground Al^{2+} ions with He atoms are plotted, as obtained by using three different trajectories; the straight-line, Coulomb, and ground-state potential trajectories. Above approximately 5 keV/u, it is obvious that the results for all channels from different trajectories agree within better than a few percent, but as the energy decreases larger deviations become apparent. In particular, the result from the Coulomb trajectory begins to deviate at an early stage. This is because the Coulomb repulsive force prohibits the colliding particles from penetrating close to each other, and hence the result obtained by this trajectory underestimates the cross section. Two sets of cross sections, obtained by straight-line and ground potential trajectories, are in good accord down to a few 100 eV/u, where a deviation between the two results begins to appear. The result using a straight line stays larger than that with the ground potential because it accounts for less repulsion. We consider that the trajectory from the ground-state potential is more realistic for colliding particles in this energy domain. The difference between the two is found to be approximately a factor of 2–3 at 100 eV/u, while the difference relative to that of the Coulomb trajectory is more than an order of magnitude. The discussion above still holds for scattering dynamics by metastable-ion impact.

For a further check, we adopted a fully quantal approach with the same MOs, and calculated electron capture as well as excitation cross sections below 100 eV/u. The present quantal results are slightly larger, but less than 5% different from those from the ground-state potential down to 80 eV/u or so. Then the deviation seems to increase as the energy decreases further. The maximum deviation between two electron-capture cross sections by the semiclassical (the ground-state potential) and quantal approaches is found to be about a factor of 2.5 at 30 eV/u. Although this amount of deviation is considered to be still tolerable for general discussion, and the ground-state potential trajectory may still be used for a reasonable estimation of the magnitude of a cross section, nevertheless it is advisable to employ a fully quantum formalism for inelastic processes below a few tens of eV/u to avoid ambiguity. In the rest of the paper, we proceed based on the result from the ground-state potential trajectory.

C. Cross sections

1. Ground state $[\mathrm{Al}^{2+}(^2S)+\mathrm{He}]$ *collisions*

Electron capture cross sections. Partial cross sections for $[\mathrm{Al}^+(^1P)+\mathrm{He}^+]$, $[\mathrm{Al}^+(^1S)+\mathrm{He}^+]$, $[\mathrm{Al}(^1D)+\mathrm{He}^+]$, $[\mathrm{Al}^+(^3P)+\mathrm{He}^+]$, and $[\mathrm{Al}^+(^3S)+\mathrm{He}^+]$ formation are shown in Fig. 4(a). At higher energies above a few tens of keV/u, the formation of the singlet manifold becomes somewhat stronger than that of the triplet manifold, although the $[\mathrm{Al}^+(^1S)+\mathrm{He}^+]$ process drops sharply above 50 keV/u. Generally, however, all channels have the same comparative magnitude in the entire energy region studied and contribute to the total cross section equally. Below 100 keV/u, the formation of channels arising from singlet and triplet manifolds mixes and interferes in a complicated manner, displaying complex oscillatory patterns. Below 1 keV/u, however, it is apparent that conspicuous peaks seen at around 0.6 and 0.8 keV/u in the $[\mathrm{Al}^+(^1D)+\mathrm{He}^+]$ channel synchronize with those in other channels at nearly the same energy, suggesting that the ladder-climbing mechanism of the flux to higher levels dominates. In the intermediate energy region from 1 to 10 keV/u, electron capture to the $[\mathrm{Al}^+(^1D)+\mathrm{He}^+]$ channel has relatively large values despite the relatively larger energy defect, in which the flux accumulates in this level through a series of ladder climbing. The $[\mathrm{Al}^+(^1P)+\mathrm{He}^+]$ channel shows a rather large peak at 50 keV/u, while its cross section decreases rather slowly below this energy. Below 1 keV/u, the magnitude of the cross sections appears to become proportional to the order of the potential level. Numerous weak structures are seen in each channel, reflecting the close and complex interference among all channels. The total cross section, the sum of all partial cross sections, is also included

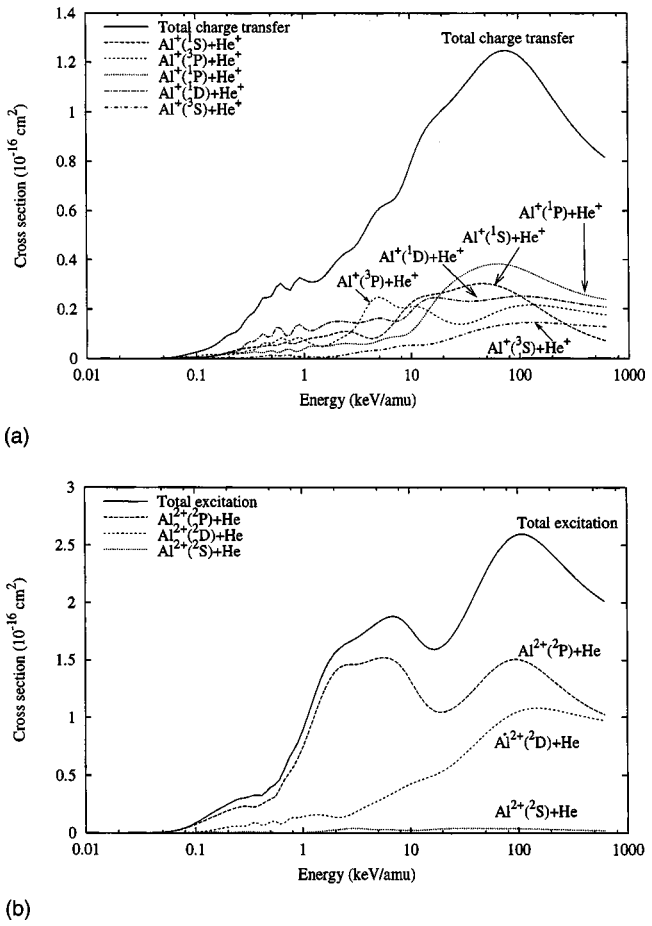

FIG. 4. Partial cross sections for (a) electron capture and (b) excitation for the ground-state $[Al^{2+}(^2S)+He]$ collision.

in Fig. 4. Since all partial cross sections become somewhat smoother above 20 keV/u or so, the total cross section is also smooth above this energy, showing an increasing trend. It has a large peak with a value of $1.25\times10^{-16}\,cm^2$ at 80 keV/u but beyond this it decreases sharply.

Excitation cross sections. Excitation cross sections are illustrated in Fig. 4(b). The $[Al^{2+}(^2P)+He]$ channel dominates in the entire energy region, while the $[Al^{2+}(^2D)+He]$ channel grows rapidly with increasing energy, but is the second in magnitude. The $[Al^{2+}(^2D)+He]$ level lies about 7.72 eV above the $[Al^{2+}(^2P)+He]$ level, and in between there are a few electron-capture channels. Hence, excitation cross sections to the $[Al^{2+}(^2D)+He]$ level should show a similar behavior to that of electron capture since the flux goes through all these intermediate channels before it gets to the $[Al^{2+}(^2D)+He]$ level. At the highest energy studied, this channel and the $[Al^{2+}(^2P)+He]$ channel become comparable in magnitude. $[Al^{2+}(^2S)+He]$ is the weakest of the three at all energies. The excitation cross sections is found to be larger by a factor of 2 than the electron capture cross section for all energies, having a value of 2.6×10^{-16} cm^2 at the maximum. The cross section for the $[Al^{2+}(^2P)+He]$ channel has two large humps at around 5 and 100 keV/u. The location of the first hump matches the peak position of the deexcitation cross section to the

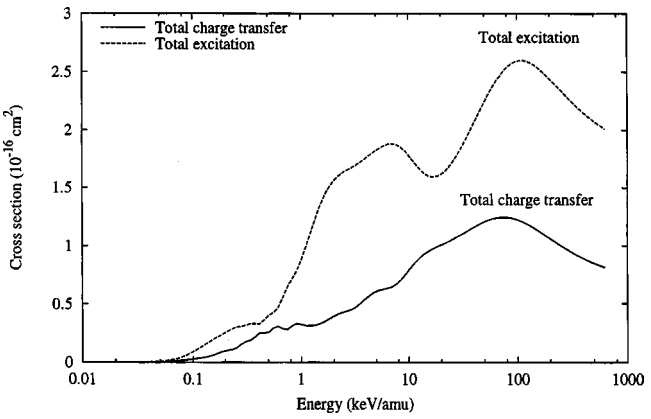

FIG. 5. Total electron-capture and excitation cross sections for the ground-state $[Al^{2+}(^2S)+He]$ collision.

$[Al^{2+}(^2S)+He]$ channel by metastable-ion impact as seen in Fig. 6 below, hence suggesting a two-step process. In contrast, the second peak at around 100 keV/u shows a similar shape to that of electron capture. Therefore the second peak is caused by the strong mixing of excitation and electron-capture channels.

As a summary, we plot both total electron-capture and excitation cross sections in the same Fig. 5. The total excitation cross section is much larger by a factor of 2, at most, than that of electron capture, and shows much stronger structures as described above.

2. Metastable state $[Al^{2+*}(^2P)+He]$ *collisions*

Electron capture cross sections. Electron-capture cross sections for this process are illustrated in Fig. 6(a) for all channels. The $[Al^+(^3P)+He^+]$ formation is the dominant channel for most energies, while $[Al^+(^1D)+He^+]$ is the second largest. Above 100 keV/u, in fact, it surpasses $[Al^+(^3P)+He^+]$ formation. The $[Al^+(^3P)+He^+]$ formation cross sections exhibit a rather smooth function with a large and broad peak near the region of 2–10 keV/u. Small but visible fluctuations are obvious for $[Al^+(^1D)+He^+]$, $[Al^+(^1P)+He^+]$, $[Al^+(^1S)+He^+]$, and $[Al^+(^3S)+He^+]$ formation in the energy region from 1 to 20 keV/u due to strong interference among them. However, no structure is found for $[Al^+(^3P)+He^+]$ formation, which is indicative that the direct one-step transition from the entrance channel dominates. It is somewhat surprising that the cross section for $[Al^+(^1S)+He^+]$ formation is the smallest, even though the energy defect between it and the initial channel is merely 0.9 eV. However, the radial couplings between the $[Al^{2+}(^2S)+He]$, $[Al^+(^1S)+He^+]$, and $[Al^+(^3P)+He^+]$ channels are very efficient for transferring flux below $R\sim6a_0$, and this is responsible for the larger cross section for $[Al^+(^3P)+He^+]$ formation. $[Al^+(^3P)+He^+]$ formation is so dominant below 10 keV/u that this process can be used as an efficient method for producing triplet Al^+ ions. The total cross section, the sum of all partial cross sections, is included in the figure. It has a broad peak around 3 keV/u with a magnitude of $1.6\times10^{-16}\,cm^2$. This value can be compared with that of ground-state collisions, with a value of

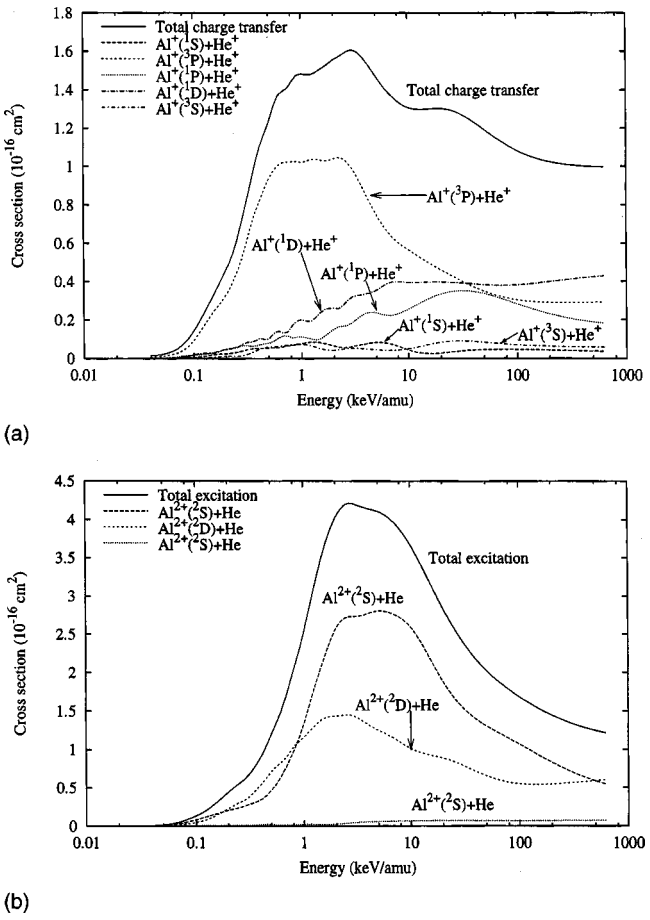

FIG. 6. Partial cross sections for (a) electron capture and (b) excitation for the metastable-state $[Al^{2+}*(^2P)+He]$ collision.

$1.25\times10^{-16}\,cm^2$. Since the energy defect between the initial and the dominant electron-capture channel is rather similar, such close values are a natural consequence.

Excitation cross sections. Excitation cross sections are displayed in Fig. 6(b). Deexcitation to the $[Al^{2+}(^2S)+He]$ channel is dominant in the energy region from 1 to 1000 keV/u, while the cross section for $[Al^{2+}(^2D)+He]$ formation becomes comparable to or slightly larger than that of

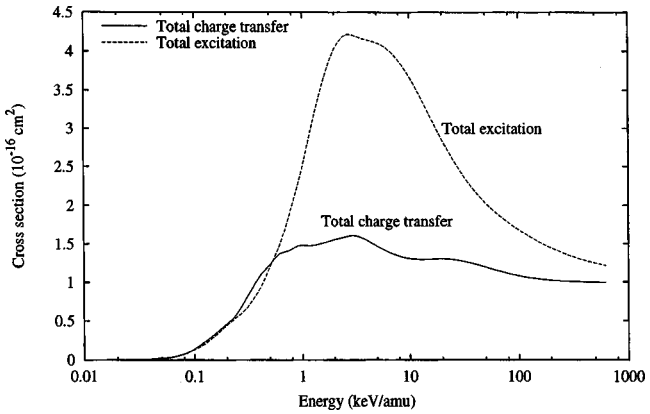

FIG. 7. Total electron-capture and excitation cross sections for the excited-state $[Al^{2+}(^2P)+He]$ collision.

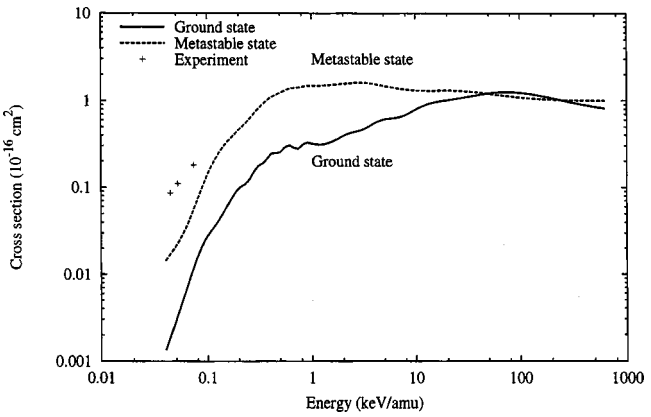

FIG. 8. Comparison of calculated electron-capture cross section with measurement [6]. Results for both ground-state and metastable-ion impacts are shown.

$[Al^{2+}(^2S)+He]$ formation between 0.2 and 1 keV/u. This feature below 1 keV/u is somewhat interesting since the energy difference between the initial and the $[Al^{2+}(^2D)+He]$ levels is larger by 1.1 eV than that between the initial and the $[Al^{2+}(^2S)+He]$ levels, and it is endothermic to reach the $[Al^{2+}(^2D)+He]$ level. A series of strong radial couplings among Σ states, which connects from the initial channel to this level at small R is very efficient, and is responsible for the effective excitation processes. The magnitude of the excitation cross section reaches $4.3\times10^{-16}\,cm^2$, which is larger by nearly a factor of 2 than that for the ground-state collisions, and the peak position shifts toward smaller energy.

As a summary, total electron-capture and excitation cross sections are plotted in Fig. 7. Similarly to the ground-state case, the excitation cross section is larger by a factor of 2 at the peak position than the electron-capture cross section, but electron capture becomes slightly larger below 0.5 keV/u. The cross sections appear to merge above 100 keV/u.

3. Comparison with experiments

In Fig. 8, the theoretical results for total electron-capture cross sections by ground-state and metastable-ion impacts are displayed with three experimental points reported by Schrey and Huber [6] for comparison. Although the present electron-capture results by the ground-state ion are in good accord with the experimental energy dependence, their magnitude is smaller than the measurement by a factor of 30. Those by the metastable ion are also smaller by a factor of 4, so even if one assumes that these metastable ions are mixed in the ion beam used in the experiment, it does not help much to improve the agreement. The present quantal results are also found to be slightly larger than those of the semiclassical method, but do not contribute much to narrowing the discrepancy. Therefore, this large discrepancy between theory and experiment is puzzling, and more experimental studies are certainly welcome to resolve the problem,

IV. CONCLUSION

We have investigated single-electron capture and excitation dynamics in collisions of Al^{2+} ions with He atoms in the

energy region from 0.05 to 1000 keV/u for both ground and excited Al^{2+} ions. The present results for electron-capture cross sections are found not to agree very well quantitatively with the measurements of Schrey and Huber below 100 eV/u. Electron-capture cross sections for the ground state are found to be comparable to those for the excited state, and this is because the energy defects between the initial and the dominant electron-capture channels for both cases are nearly equal. On the other hand, excitation cross sections for the two cases are found to be quite different. We have also examined the effect of the heavy-particle trajectory. We have found that trajectories based on the straight line and the ground-state potential give nearly identical results for electron capture down to 100 eV/u, while significant deviations begin to emerge below a few tens of eV/u, at which point a fully quantum-mechanical approach should be employed. Although adiabatic potentials and couplings based on the MRD-CI method are found to be more accurate in absolute value, the ALCHEMY approach gives reasonable relative values for the adiabatic potentials, and for cross-section calculations the two approaches agree within a few percent at energies.

ACKNOWLEDGMENTS

The work was supported in part by a Grant-in-Aid from The Ministry of Education, Science, Technology, Sport and Culture, Japan (M.K.). The financial support of the Deutsche Forschungsgemeinschaft (Grant No. Bu 450/6-3) and the Fonds der Chemischen Industrie is also gratefully acknowledged (J.P.G., G.H., and R.J.B.). M.K. was also supported by JSPS.

[1] M. Kimura, A. B. Sannigrahi, J. P. Gu, G. Hirsch, and R. J. Buenker, Astrophys. J. **473**, 1114 (1996).
[2] C. M. Dutta, P. Nordlander, and M. Kimura, Chem. Phys. Lett. **264**, 51 (1997).
[3] M. Kimura, J. P. Gu, G. Hirsch, R. J. Buenker, A. Domondon, T. Watanabe, and H. Sato, Phys. Rev. A **56**, 1892 (1997).
[4] M. Kimura, C. M. Dutta, P. Nordlander, J. P. Gu, G. Hirsch, and R. J. Buenker, Phys. Rev. A **59**, 405 (1998).
[5] J. P. Gu, G. Hirsch, R. J. Buenker, M. Kimura, C. M. Dutta, and P. Nordlander, Phys. Rev. A **62**, 0527201 (2000).
[6] H. Schrey and B. A. Huber, J. Phys. B **14**, 3197 (1981).
[7] M. Kimura and N. F. Lane, Adv. At., Mol., Opt. Phys. **26**, 76 (1989).
[8] A. D. McLean, M. Yoshimine, B. H. Lengsfield, P. S. Bagus, and B. Liu, ALCHEMY II (IBM, 1981).
[9] R. J. Buenker and S. D. Peyerimhoff, Theor. Chim. Acta **35**, 33 (1974); **39**, 217 (1975); R. J. Buenker, Int. J. Quantum Chem. **29**, 435 (1986); S. Krebs and R. J. Buenker, J. Chem. Phys. **103**, 5613 (1995).
[10] R. J. Buenker, in *Proceedings of the Workshop on Quantum Chemistry and Molecular Physics, Wollongong, Australia*, edited by P. G. Burton (Wollongong University Press, Wollongong, 1980); in *Studies in Physical and Theoretical Chemistry*, edited by R. Carbo, Vol. 21 of *Current Aspects of Quantum Chemistry* (Elsevier, Amsterdam, 1981), p. 17; R. J. Buenker and R. A. Phillips, J. Mol. Struct.: THEOCHEM **123**, 291 (1985).
[11] G. Hirsch, P. J. Bruna, R. J. Buenker, and S. D. Peyerimhoff, Chem. Phys. **45**, 335 (1980).
[12] J. M. O. Matos, P.-A. Malmqvist, and B. O. Roos, J. Chem. Phys. **86**, 5032 (1987).
[13] K. K. Sunil, J. Lin, H. Siddiqui, P. E. Siska, K. D. Jordan, and R. Shepard, J. Chem. Phys. **78**, 6190 (1983).
[14] D. E. Woon and T. H. Dunning, Jr., J. Chem. Phys. **100**, 2975 (1994).
[15] E. Clementi and C. Roetti, At. Data Nucl. Data Tables **14**, 177 (1974).
[16] T. G. Winter and N. F. Lane, Phys. Rev. A **17**, 66 (1978).
[17] S. Bashkin and J. O. Stoner, Jr., *Atomic Energy Levels and Grotrian Diagrams* (North-Holland, Amsterdam, 1975).